JOURNAL OF AIRCRAFT
Vol. 43, No. 1, January–February 2006

Experimental and Analytical Study of Blade Lag Damping Augmentation Using Chordwise Absorbers

Hao Kang,* Edward C. Smith,† and George A. Lesieutre‡
Pennsylvania State University, University Park, Pennsylvania 16802

The feasibility of helicopter blade lag damping using embedded chordwise absorbers is investigated both analytically and experimentally. The basic feature of this approach is the use of tuned damped absorbers along the blades. This concept, utilizing a portion of the leading-edge weights that are already incorporated into the blade as a portion of the mass of the absorbers, can have the potential to replace or augment current blade lag dampers and reduce the complexity, aerodynamic drag, and weight of the rotor hub. The analysis is performed using an aeromechanical stability analysis program developed using the finite element method for the rotor system with blades incorporating absorbers. The test is conducted using a small-scale hingeless rotor with a single absorber on each blade. Parametric studies for blade lag damping augmentation with various absorber mass, location, damping, and tuned frequency are also presented. The analytical and experimental results show that blade damping augmentation using chordwise absorbers varies from 0.3 to 15% critical damping depending on the blade and the absorber parameters. The analytical results also show that the damping augmentation improves the ground-resonance stability of the rotor system.

Nomenclature

h	=	vertical distance from fuselage center of gravity to hub center
$\boldsymbol{I}, \boldsymbol{J}, \boldsymbol{K}$	=	inertial coordinate system vectors
K	=	absorber spring complex stiffness
k'	=	absorber spring stiffness
m_a	=	absorber mass, % of blade mass
R	=	blade radius
t	=	time
u, v, w	=	absorber displacements in blade axial, lag, and flap directions
x	=	radial blade station
$x_{\mathrm{CG}}, y_{\mathrm{CG}}$	=	hub center position relative to fuselage center of gravity
α_s	=	fuselage pitch angle (positive nose down)
β_p	=	blade precone
ζ	=	blade lag angle
η	=	absorber spring loss factor
θ_0	=	blade geometry pitch angle
ν_a	=	nondimentional absorber frequency
ν_{a0}	=	nonrotating absorber frequency
ν_ζ	=	nondimentional blade lag frequency
ϕ	=	blade elastic twist
ϕ_s	=	fuselage roll angle (positive advancing side down)
χ	=	absorber displacement
χ_0	=	initial absorber displacement
ψ	=	blade azimuth
Ω	=	nominal rotor speed
$\dot{(\,)}$	=	$\partial(\,)/\partial t$
$(\,)'$	=	$\partial(\,)/\partial x$

Introduction

AEROMECHANICAL instabilities such as ground and air resonance are major design considerations for articulated and soft in-plane hingeless rotors. When controlled with fuselage system damping, the inclusion of damping in the blade lag mode is an efficient method for avoiding these instabilities.[1] There are many successful approaches to providing lag damping in the rotor system. Among these are elastomeric, hydraulic, and fluidlastic dampers. These approaches, however, add weight, complexity, maintenance, and aerodynamic drag to the rotor hub.

Recently, many new rotor blade damping approaches have been investigated, including constrained layer damping treatment,[2,3] active constrained layer damping treatment,[4,5] enhanced active constrained layer damping treatments,[6] magnetorheological fluid dampers,[7,8] and electrorheological fluid dampers.[9] Some approaches showed potential applications for rotor systems, but more detailed studies are required before any conclusive strategy for lag damping is proposed.[10]

Rotor blade lag damping using embedded chordwise absorbers provides an alternative approach for blade lag damping augmentation.[11] This approach uses the tuned chordwise absorbers along the blades. This approach utilizes a portion of the blade leading-edge weights that are already incorporated into the blade as a portion of the absorber masses. It can replace the current blade lag dampers and reduce the complexity and the aerodynamic drag of the rotor hub.

The concept of blade lag damping using chordwise absorbers was first studied by one of the authors and his coresearchers in Ref. 11. A simple blade-like beam under a tensile load with tuned absorbers distributed spatially and in frequency was analytically examined. The beam damping results showed that 3∼8% critical damping could be obtained for different tuning bands with a small mass addition. In the analysis, the dynamic stiffness approach was used to model the highly distributed absorbers.

In Ref. 12, the authors further investigated the concept of blade lag damping using chordwise absorbers. A blade with properties similar to the Blackhawk helicopter rotor blade was analyzed with highly distributed chordwise absorbers. The highly distributed absorber system was modeled using frequency-dependent complex distributed masses. The numerical results showed that the absorbers, highly distributed both in space and in frequency, could be very effective at providing damping in the blade lag mode. Using as little as 3% of the total blade mass, 4% critical damping in the blade lag mode was achieved.

In previous research, the absorber was modeled using either a frequency-dependent mass model or a dynamic stiffness model. The blade was modeled using a simple beam undergoing lag bending. Clearly, a comprehensive analysis of the coupled

Received 8 April 2005; accepted for publication 16 April 2005.

*Graduate Research Assistant; currently Research Scientist, Advanced Rotorcraft Technology, Inc., Mountain View, California.
†Professor. Member AIAA.
‡Professor. Associate Fellow AIAA.

blade-fuselage-absorber dynamic system needs to be developed to systematically investigate the blade lag damping using chordwise absorbers. In addition, experimental verification needs to be conducted to determine the feasibility of the concept.

The objective of this paper is to further study the blade lag damping using embedded chordwise absorbers. The lag damping of the blade incorporating the chordwise absorber is measured. A fully coupled blade-fuselage-absorber dynamic model is developed. The fuselage pitch and roll, the blade flap bending, lag bending, elastic twist, and the absorber motion are taken into account. Using the model, the blade lag damping augmentation is addressed. The effects of the absorber and blade parameters are discussed. The ground resonance stability of a rotor system with chordwise absorbers is examined.

Analytical Model

The blade-fuselage-absorber dynamic model is schematically shown in Fig. 1. It includes elastic blades, a fuselage, and discrete absorbers. The fuselage is modeled as a rigid body with pitch and roll rotations about the center of gravity. The rotor blade is modeled as a slender elastic beam undergoing flap bending, lag bending, elastic twist, and axial deflection. The blade is embedded with discrete chordwise absorbers. Each absorber is modeled using a mass-spring pair and is assumed to move in the chordwise direction of the blade only. Blade element theory is used to compute the quasi-steady aerodynamic loads. The rotor inflow is assumed to be uniform.

The equations governing the motion of the rotor, fuselage, and absorbers are given using the generalized form of Hamilton's principle by

$$\delta \prod = \int_{t_1}^{t_2} (\delta T - \delta U + \delta W) \tag{1}$$

where δT is the variation of kinetic energy and δU is the variation of strain energy. The variations of the kinetic energy and the strain energy include the contributions from the blades, the absorbers, and the fuselage. δW is the virtual work caused by the aerodynamic forces. Details of the virtual energy expressions of the blades and the fuselage are presented in Ref. 10.

Assuming that the absorber moves in the blade chordwise direction only, the variation of strain energy of the absorbers can be given by

$$\delta U_a = \sum_{m=1}^{N_b} \sum_{n=1}^{N_a} K_{m,n} \chi_{m,n} \delta \chi_{m,n} \tag{2}$$

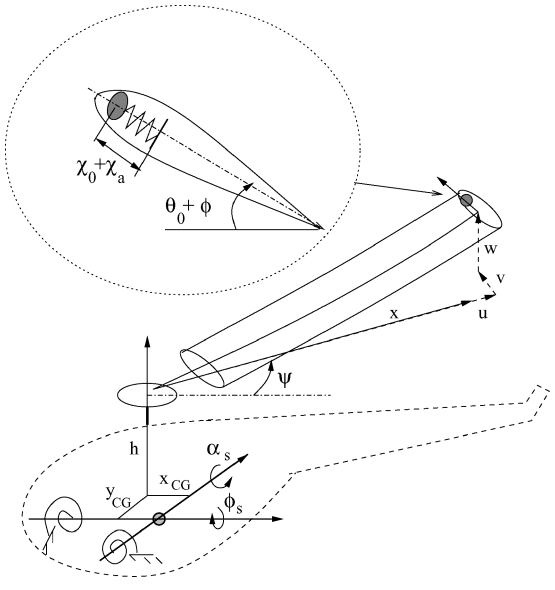

Fig. 1 Rotor-fuselage-absorber model.

where N_a is the number of the discrete absorbers on one blade and N_b is the number of blades. For an absorber with an elastomeric material spring, the spring stiffness can be expressed using a complex number.

$$K_{m,n} = k'_{m,n}(1 + i\eta_{m,n}) \tag{3}$$

The variation of kinetic energy of the chordwise absorbers can be written as

$$\delta T_a = \sum_{m=1}^{N_b} \sum_{n=1}^{N_a} (m_a)_{m,n} \boldsymbol{V}_{m,n} \delta \boldsymbol{V}_{m,n} \tag{4}$$

where $\boldsymbol{V}_{m,n}$ is the velocity of the nth absorber on the mth blade. It can be expressed as

$$\boldsymbol{V}_{m,n} = V_x \boldsymbol{I} + V_y \boldsymbol{J} + V_z \boldsymbol{K} \tag{5}$$

where

$$V_x = -\dot{\alpha}_s h - \alpha_s \dot{z}_a + \alpha_s \phi_s x_a \cos\psi - y_a \cos\psi + \dot{x}_a \cos\psi - \beta_p \dot{z}_a \cos\psi - x_a \sin\psi - \dot{y}_a \cos\psi + \beta_p z_a \sin\psi \tag{6}$$

$$V_y = \dot{\phi}_s h + \phi_s \dot{z}_a + x_a \cos\psi + \dot{y}_a \cos\psi - \beta_p z_a \cos\psi + \dot{x}_a \sin\psi - y_a \sin\psi - \beta_p \dot{z}_a \sin\psi \tag{7}$$

$$V_z = -\dot{\phi}_s y_{cg} + \dot{\alpha}_s x_a \cos\psi - \phi_s x_a \cos\psi - \alpha_s y_a \cos\psi + \dot{\alpha}_s x_{cg} + \phi_s \dot{y} \cos\psi - \alpha_s x_a \cos\psi - \phi_s x_a \sin\psi + \phi_s \dot{y}_a \cos\psi - \alpha_s y_a \sin\psi + \dot{z}_a \tag{8}$$

Here x_a, y_a, and z_a are the three components of the position vector of the absorber in the undeformed blade frame. They are defined as

$$x_a = x + u - \lambda\phi' - v'(\chi_a + \chi_0)\cos(\theta_0 + \phi) - w'(\chi + \chi_0)\sin(\theta_0 + \phi) \tag{9}$$

$$y_a = v + (\chi + \chi_0)\cos(\theta_0 + \phi) \tag{10}$$

$$z_a = w + (\chi + \chi_0)\sin(\theta_0 + \phi) \tag{11}$$

The equations of motion of the rotor-fuselage-absorber system are spatially discretized using the finite element method. Each beam-absorber element consists of 15 degrees of freedom describing the motion of the beam element and 1 degrees of freedom describing the motion of the embedded absorber. The equations of motion are then linearized about the trim position to obtain the perturbation equations. The perturbation blade and absorber equations for the individual blades and absorbers are transformed to the nonrotating coordinate system to give the final rotor, fuselage, and absorber equations. Solution of the complex eigenvalue problem of the homogeneous rotor, fuselage, and absorber equations yields the modal frequencies and damping.

Experiment Description

To validate the analytical techniques developed to predict the blade lag damping and verify the blade lag damping using embedded chordwise absorbers, a small-scale model rotor test was performed. The test was conducted using a 39 in diameter, two-bladed hingeless soft-in-plane rotor. The blade was a rigid steel rod and was mounted to the hub using a root lag flexure. The flexure was designed so that the flap and torsion stiffness of the blade were much higher than the lag stiffness. Thus, the lag-flap and lag-torsion couplings were very small. To examine the effects of the blade lag frequency, two sets of root lag flexure were used in the test. The detailed properties of the model blade are given in Table 1.

Figure 2 shows the overall view of the model rotor blade test. The rotor hub was supported by a gimbaled fuselage. The gimbaled fuselage was free to rotate in two directions, which represent the pitch and roll motion of the fuselage. Flexure beams mounted across

Table 1 Blade properties

Rotor properties	
Number of blades	2
Radius, in.	19.5
Chord, in.	0.5
Mass, slug	0.0155
Rotating speed, rpm	0–300
Nonrotating lag frequency, Hz	6.5[a], 4[b]
Lag damping, % critical damping	0.3

[a]Rotor configuration I. [b]Rotor configuration II.

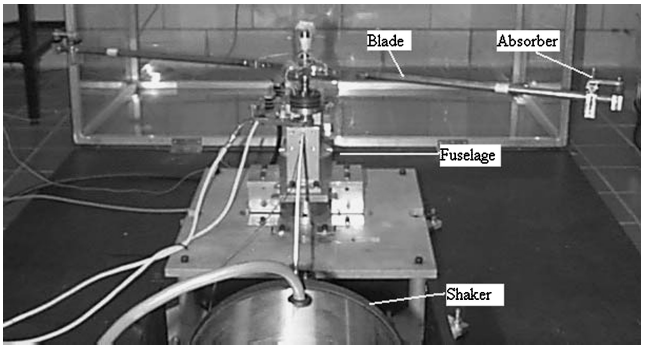

Fig. 2 Blade lag damping test.

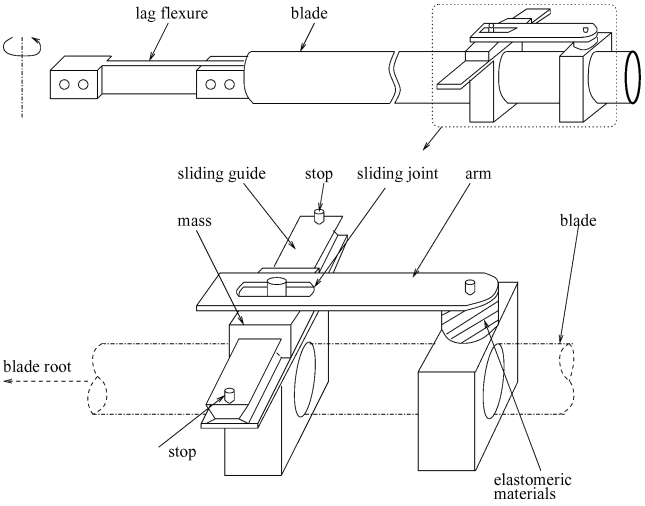

Fig. 3 Blade and absorber.

the fuselage gimbal and in between the body and the stand provide the pitch and roll stiffnesses of the body.

Figure 3 shows an expanded view of the blade and the absorber used in the test. The absorber consisted of a mass, an elastomeric torsional spring, a sliding guide, a short arm, and some supporting parts. The sliding guide was fixed on the blade perpendicular to the blade axis. The mass was supported on the sliding guide so that it could slide along the guide in the lag direction. There were two adjustable stops on the sliding guide. These stops were used to lock the mass for baseline test cases (without the effects of the absorber). The mass was also linked with one end of the short arm through a sliding joint. On the other end of the short arm, there was an elastomeric torsional spring, which was used as the spring and damping elements of the absorber. The shear modulus of the elastomeric material used in the present tests was 30 psi with 0.27 loss factor. This absorber configuration was designed so as to generate the soft spring required for low tuning frequencies (6∼9 Hz). The absorber can be fixed at any radial position on the blade.

Two sets of blade lag damping tests were conducted. The first was the nonrotating blade lag damping test. The second was the rotating blade lag damping test. The nonrotating blade test was conducted in order to get an initial understanding of the frequency and damping characteristics of the blade with the chordwise absorbers. In the nonrotating test, the hub was fixed, and the tip of the blade was mounted to a static stand through a tensile spring. The tensile load that the tensile spring provides can be adjusted by changing the distance between the blade tip and the stand. The tensile load was used as the primary variable in the experiment. The blade root flexure was instrumented with a strain gauge bridge to measure the blade lag deflection. For each tensile load, the blade tip was held by hand with a static lag deflection. Then, the blade was released and the lag motion of the blade was allowed to decay freely. The transient decay of the blade lag motion was recorded and used to identify the blade lag frequency and damping.

In the rotating blade test, rotor speed was used as the primary variable. At each rotation speed, the lead-lag regressive mode was excited using a shaker. The shaker was mounted at the base of the stand and connected to the gimballed body. It oscillated the body about its pitch axis at the lead-lag regressive frequency. When sufficient blade lead-lag amplitude was achieved, the shaker was stopped, and a clamp was used to lock out the motion of the body, which allowed the motions of the blade to freely decay. A differential lead-lag signal was obtained by subtracting the lead-lag signal of one blade from the other to eliminate drive-system coupling effects from the data. The lead-lag modal frequency and damping were identified from the differential lead-lag signal by performing a moving-block analysis on the transient decay of the blade motions.

Results and Discussion

Blade Lag Damping Correlation

The lag damping of the nonrotating blade under the tensile loads was measured for two absorber locations, $0.5R$ and $0.85R$. For each absorber location, the damping was measured with locked and released absorbers. The damping augmentation caused by the absorber was obtained by subtracting the damping data of the blade with the locked absorber from the data with the released absorber. The absorber mass was 7.1% of the blade mass, the absorber frequency was 8.9 Hz, and the loss factor was 0.38.

The blade lag damping measurements for the two absorber locations are shown as functions of the blade lag frequency (tensile load) in Fig. 4. The results for the locked absorber case are also shown as the baseline in the figure. It represents the structural damping of the blade. For the blade with the released absorber, significant damping augmentation exists in the blade lag mode. The damping augmentation increases as the blade lag frequency increases and approaches the absorber frequency. For the blade with an absorber at $0.85R$, the blade lag damping varies from 0.5 to 7.5% critical damping, depending on the blade lag frequency. For the blade with an absorber at $0.5R$, the blade lag damping varies from 0.3 to 2.7%

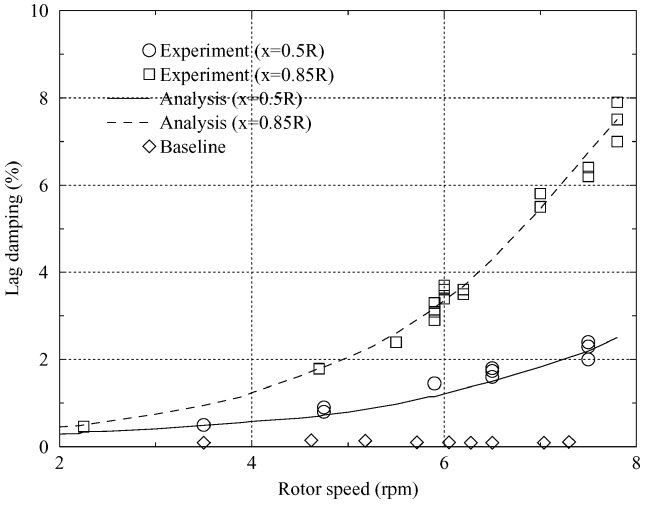

Fig. 4 Experimental and analytical blade lag damping.

Table 2 Absorber properties for rotating blade lag damping test

No	Mass, %	Frequency, Hz	Loss factor	Location, r/R
2	8.4	6.3	0.41	0.5 and 0.85
3	9.7	5.5	0.42	0.5 and 0.85

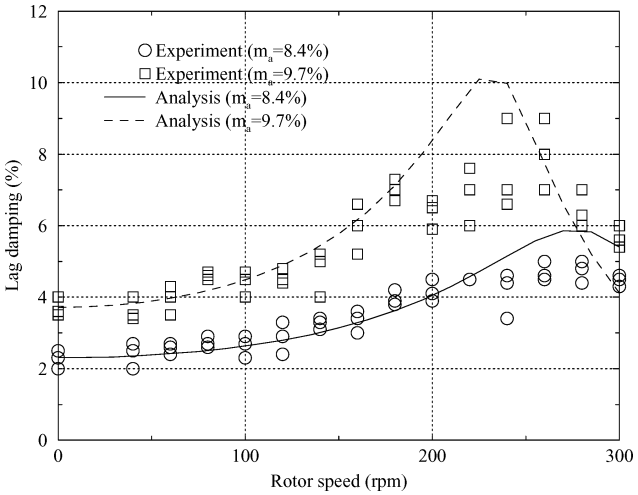

Fig. 5 Blade lag damping for rotor configuration I and absorber at 0.85*R*.

critical damping as the blade lag frequency increases. The analytical results are also presented in the figure. They show good agreement with the measured data.

The experimental and analytical results of the nonrotating blade lag damping initially verify that significant blade lag damping augmentation can be achieved using the chordwise absorber and that blade lag damping augmentation depends on the absorber location. Further tests and analyses were then conducted for the rotating blade.

Two rotor-blade configurations and two sets of absorbers were used in the rotating blade test. The rotor blade configurations, I and II, had different blade root lag flexure and, thus, had different lag frequencies. The nonrotating lag frequencies for configurations I and II were 6 and 4 Hz (without absorber), respectively. The two sets of absorbers represented the various absorber masses and tuning frequencies. The properties of the absorbers are shown in Table 2. For each test case, the measurement was made with locked and released absorbers. The damping augmentation caused by the application of the absorber was obtained by subtracting the damping data of the blade with the locked absorbers from the corresponding data with the released absorbers.

For rotor configuration I, the measured blade lag damping augmentation vs rotor speed is shown in Fig. 5 for the absorber at $0.85R$ and in Fig. 6 for the absorber at $0.5R$. Although the blade lag damping data have considerable scatter, significant damping augmentation can be observed. The blade lag damping increases first and then decreases as the rotor speed increases. As shown in Fig. 5, using an absorber with 9.7% blade mass at $0.85R$, the blade lag damping augmentation varies from 4% to 9% critical damping with the change in rotor speed. The blade lag damping augmentation varies from 2.3% to 6% critical damping for the case, where the absorber mass is 8.4% of the blade mass. For the absorber at $0.5R$, lower blade lag damping augmentation is measured as shown in Fig. 6. The damping augmentation varies from 1% to 7.3% critical damping for the case where the absorber mass is 9.7% of the blade mass and from 1.8% to 3.8% critical damping for the case where the absorber mass is 8.4% of the blade mass.

The damping augmentation vs rotor speed for rotor configuration II is shown in Figs. 7 and 8. Compared to the augmentation for rotor configuration I, much lower blade lag damping augmentation exists for rotor configuration II. Even with the absorber at $0.85R$, only 0.7% to 1.9% critical damping is augmented in the blade lag mode. The results show that the blade lag frequency has a significant influence on blade lag damping augmentation using chordwise absorbers. The analytical results are also shown in the figures. They show the same trend and augmentation as the experimental data.

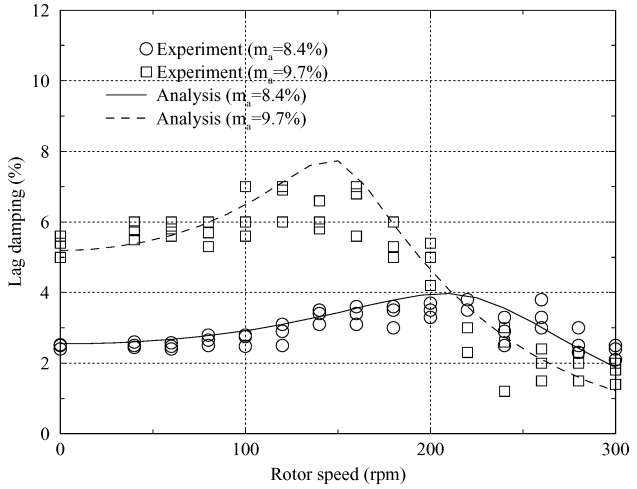

Fig. 6 Blade lag damping for rotor configuration I and absorber at 0.5*R*.

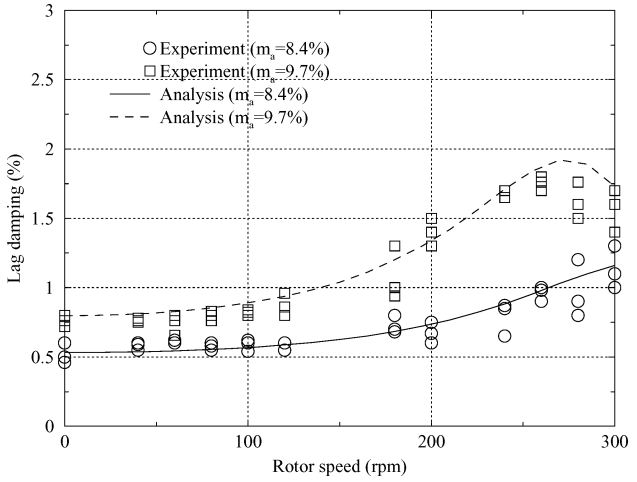

Fig. 7 Blade lag damping for rotor configuration II and absorber at 0.85*R*.

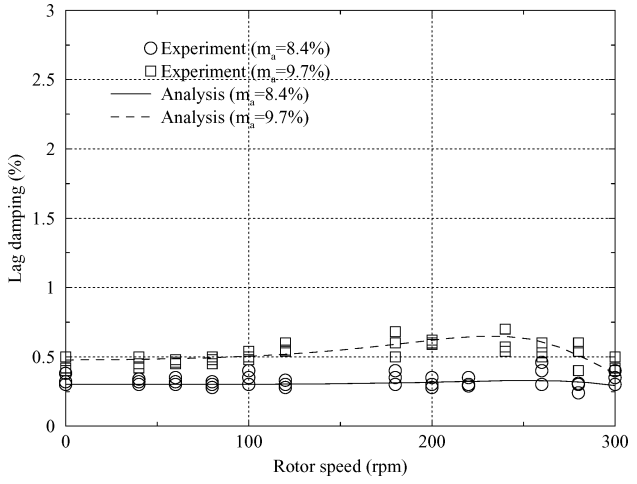

Fig. 8 Blade lag damping for rotor configuration II and absorber at 0.5*R*.

Parametric Effects

A rotor model similar to the AFDD hingeless rotor blade was used as the baseline rotor for the parametric study on blade damping. The properties of the AFDD rotor are given in Ref. 13. In the analysis, it

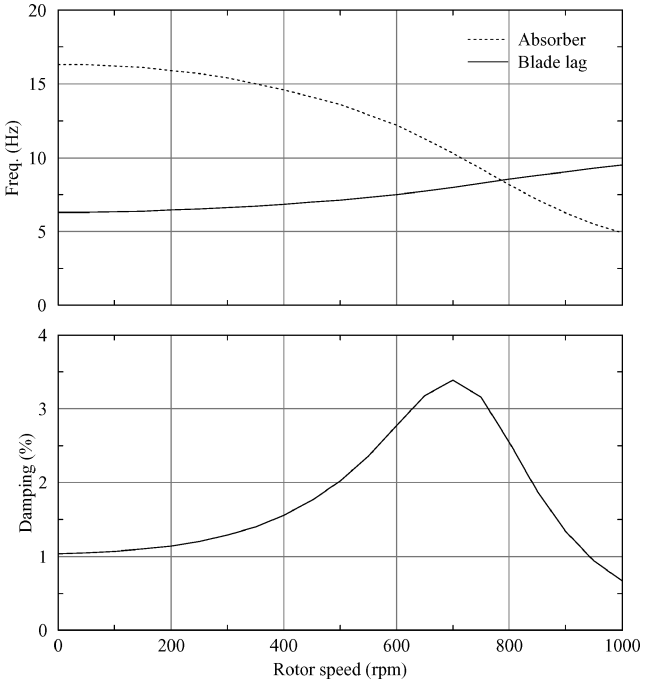

Fig. 9 Blade lag and absorber dynamic characteristics.

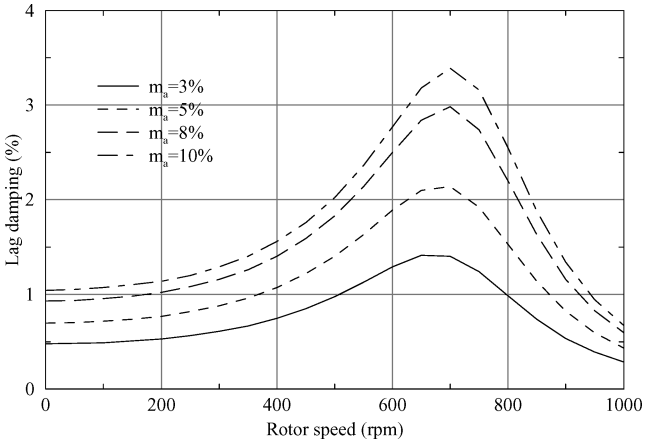

Fig. 10 Effects of absorber mass.

is assumed that there is no blade aerodynamic damping or structural damping.

For a blade with a single absorber at the tip of the blade, the fundamental blade lag frequency and damping and the absorber frequency are shown in Fig. 9 as functions of the rotor speed. The mass of the absorber is 10% of the blade mass. The loss factor of the absorber spring is 0.5. The absorber nonrotating frequency is 0.84Ω. The nominal rotor speed of the AFDD rotor, Ω, is 1000 rpm. As shown, the absorber frequency decreases, and the fundamental blade lag frequency increases as the rotor speed increases. This is because the centrifugal force provides a geometric stiffness to the blade lag motion, but softens the effective stiffness of the absorber. At a speed of 815 rpm, the frequency of the absorber is close to the blade lag frequency. The blade lag damping increases as the absorber frequency approaches the blade lag frequency. At a rotor speed of 780 rpm, the blade lag damping reaches a maximum value of 3.5% critical damping. The blade lag damping decreases when the rotor speed increases further.

The effects of the absorber mass on the blade lag damping are shown in Fig. 10. The blade lag damping for four different absorber masses (3%, 5%, 8%, and 10% of the blade mass) are compared for a blade tip absorber and a zero-blade-pitch-angle case. As shown, the maximum damping increases from 1.3% to 3.5% critical damping as the absorber mass varies from 3% to 10% of the blade mass.

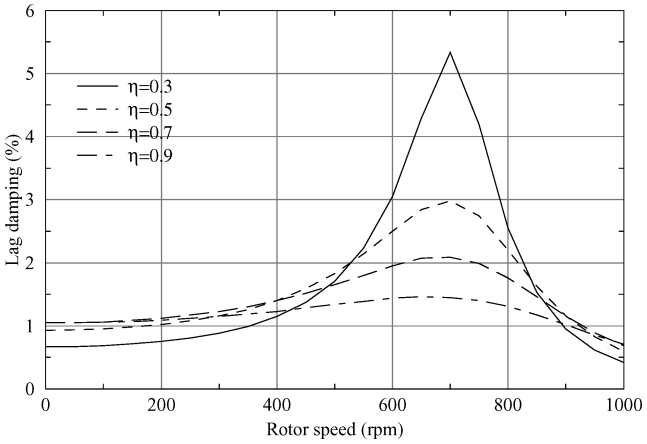

Fig. 11 Effects of loss factor.

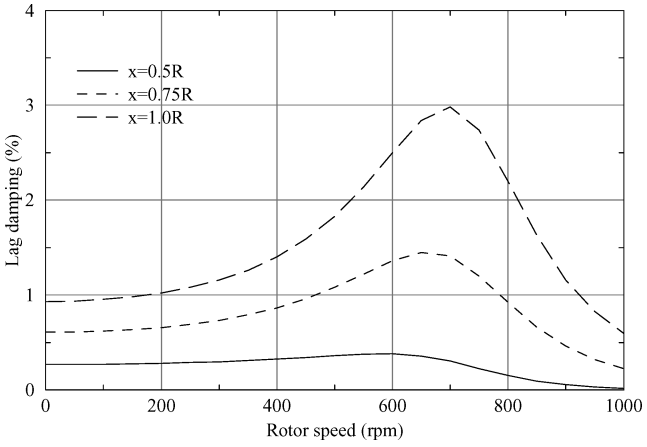

Fig. 12 Effects of absorber position.

A comparison of the blade lag damping is given in Fig. 11 for four different absorber spring loss factors: 0.3, 0.5, 0.7, and 1.0. The blade lag damping is calculated for zero blade pitch angle and a blade tip absorber with 8% blade mass. The absorber nonrotating frequency is 0.84Ω. As shown, the lower the absorber spring loss factor, the higher the maximum blade lag damping. For an absorber spring loss factor of 0.3, the maximum damping of the blade lag mode is 5.4% critical damping.

The effect of the absorber locations on the blade lag damping augmentation is shown in Fig. 12. The blade lag damping vs rotor speed for three different absorber locations ($1.0R$, $0.75R$, and $0.5R$) is compared in the figure. For all three cases, the mass of the absorber is 8% of the blade mass. The nonrotating frequency of the absorber is 0.84Ω, and the loss factor is 0.5. As shown, the blade lag damping increases as the absorber approaches the blade tip. The lag damping for the blade with the tip absorber is approximately two times the damping with an absorber at $0.75R$ and six times the damping with an absorber at $0.5R$.

At the beginning of this section, it was observed that the absorber tuning frequency decreases and the blade lag frequency increases as the blade rotor speed increases. At a certain speed, the frequency of the absorber is close to the blade lag frequency. At this "tuned" rotation speed, the blade lag mode has maximum damping augmentation. Therefore, the variation of the absorber natural frequency will change the rotation speed when the absorber is tuned to the blade lag frequency. This means that the effective damping augmentation will be shifted as the absorber natural frequency changes. This can been verified by the results for different absorber frequencies shown in Fig. 13. The mass of the blade-tip absorber is 8% of the blade mass, and the loss factor is 0.5. As shown, the blade lag damping increases from 2.4% to 15% critical damping when the nonrotating absorber frequency decreases from 0.84Ω to 0.45Ω.

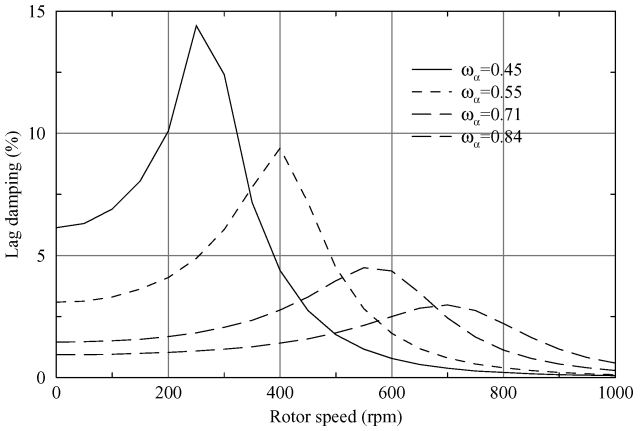

Fig. 13 Effects of absorber tuning frequency.

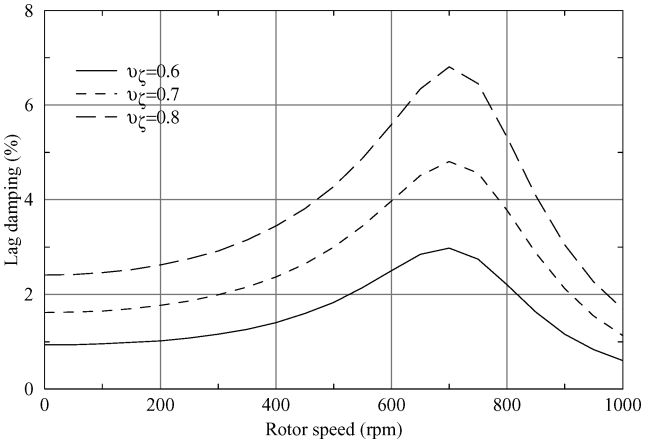

Fig. 14 Effects of blade lag frequency.

Similarly, the blade lag frequency has an influence on the blade lag damping augmentation. This influence can be observed from the blade lag damping augmentation for different blade lag stiffnesses as shown in Fig. 14. The blade lag frequencies at the nominal rotor speed are 0.6Ω, 0.7Ω, and 0.8Ω. For different blade lag frequencies, the absorber frequency is determined so that the tuned rotation speed (i.e., where the frequency of the absorber and the blade lag mode are close) remains the same. As shown, the maximum blade lag damping increases from 2.4% to 7% critical damping when the blade lag frequency increases from 0.6Ω to 0.8Ω.

Ground-Resonance Stability

As an example of applying the chordwise absorber for the blade lag damping augmentation, the ground resonance stability of a rotor system was examined. The rotor system consisted of a rotor with three hingeless blades and a fuselage with pitch and roll degrees of freedom. At the tip of each blade, there was a chordwise absorber. In the examination, the rotor system with the locked chordwise absorbers was used as the baseline rotor system. The detailed properties of the rotor system are tabulated in Table 3.

The ground resonance stabilities of the baseline rotor system and the rotor system with the released absorbers are shown in a Coleman diagram in Fig. 15. The system frequencies in the fixed frame presented in the figure are the blade progressive and regressive lag frequencies ($1+\nu_\zeta$ and $1-\nu_\zeta$), body pitch and roll frequencies ($\omega_{\alpha s}$ and $\omega_{\phi s}$), and the absorber progressive and regressive frequencies ($1+\nu_a$ and $1-\nu_a$). The blade lag damping vs rotor rotation speed is also shown in the figure. For the baseline rotor system, ground resonance appears at the resonance of the fuselage roll motion and the regressive lag mode over the rotation speed range from 620 to 800 rpm, where the blade regressive lag mode has negative damping. As the absorbers on each blade of the rotor are released and the absorber frequency is tuned to the system resonance frequency in the unstable rotation speed range from 620 to 800 rpm, the blade regressive lag mode damping is augmented. For the considered rotor system, the minimum blade lag damping is increased from -0.6 to 0.2 using the absorbers with 10% blade mass, 0.5 loss factor, and a frequency of 0.84Ω. The rotor system is stabilized.

Table 3 Rotor properties for ground-resonance stability analysis

Properties		
Rotor		
Number of blades N_b		3
Radius R, in.		31.92
Chord c, in.		1.65
Hinge offset e, in.		3.35
Mass, slug		0.0143
Hub height above c.g. h, in.		9.49
Lock number		7.37
Blade flap inertia, lb-in.^{2}		59.01
Nonrotating flap frequency, Hz		3.13
Nonrotating lag frequency, Hz		6.70
Lag damping, % critical damping		0.52
Fuselage		
	Roll	Pitch
Inertia, slug-in.^{2}	20.36	70.42
Frequency, Hz	4.00	2.00
Damping, % critical damping	0.93	3.20

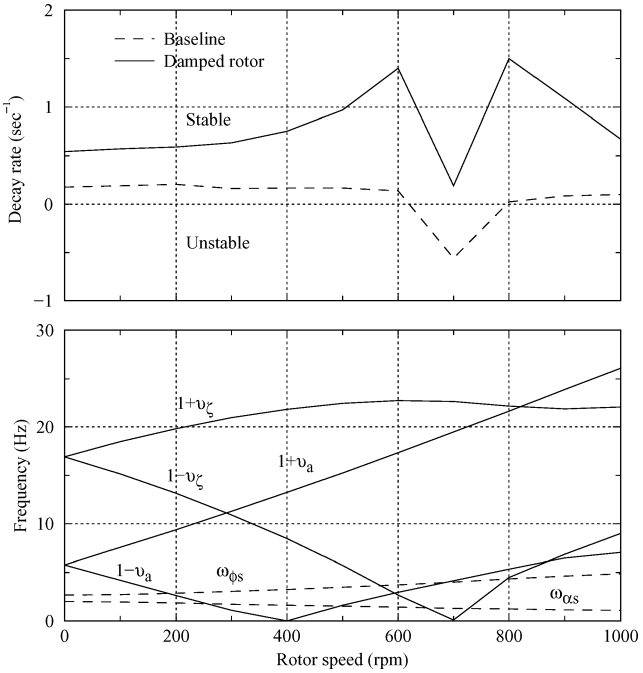

Fig. 15 Ground-resonance stability of rotor system with embedded absorbers.

Conclusions

The feasibility of helicopter blade lag damping using chordwise absorbers has been investigated. A set of blade lag damping tests has been conducted. A comprehensive aeromechanical stability analysis of the rotor-fuselage-absorber system has been developed. Parametric studies of the blade lag damping using a chordwise absorber have been performed. Ground resonance stability of a rotor system with chordwise absorbers has been examined. The following conclusions were drawn:

1) For a blade with chordwise absorbers, the blade lag frequency increases, and the absorber frequency decreases as the rotor speed increases. At a certain rotation speed, the absorber is tuned to the blade lag frequency. The blade lag damping augmentation increases and reaches a maximum value as the absorber tends to the blade lag mode. The blade lag damping using the chordwise absorbers demonstrates an effective damping range in rotation speed.

2) Both the theoretical and experimental results show promising blade lag damping augmentation using chordwise absorbers. The blade damping augmentation using chordwise absorbers can be as much as 15% critical damping, depending on the blade and the absorber parameters.

3) Blade lag damping augmentation using chordwise absorbers depends on the chordwise absorber mass, location, spring loss factor, and tuned frequency. Increasing absorber mass increases the blade lag damping augmentation. Increasing absorber loss factor decreases the blade lag damping augmentation. Blade lag damping augmentation increases as the absorber radial position moves from inboard to the tip of the blade. The blade lag damping augmentation also changes as the absorber natural frequency changes.

4) Blade lag damping augmentation highly depends on the blade lag frequency. Increasing the blade lag stiffness increases the blade lag damping augmentation.

5) The blade lag damping augmentation using chordwise absorbers improves the ground resonance stability of the rotor system.

Acknowledgment

This research was carried out with support from the Lord Corporation (technical monitor: Guy Billoud).

References

[1]Johnson, W., *Helicopter Theory*, Dover, Mineola, NY, 1994, pp. 668–693.

[2]Smith, C. B., and Wereley, N. M., "Passive Damping Techniques for Composite Rotorcraft FlexBeams," *Proceedings of the 36th AIAA/ASME/ASCE/AHS/ASC Structures, Structural Dynamics, and Materials Conference and Exhibit, and AIAA/ASME/AHS Adaptive Structures Forum*, April 1995, pp. 684–689; also AIAA Paper 95-1232, April 1995.

[3]Wang, G., and Wereley, N. M., "Frequency Response of Beams with Passively Constrained Damping Layers and Piezo-Actuators," *Proceedings of the 5th SPIE Symposium on Smart Structures and Materials, Passive Damping and Isolation Conference*, edited by L. Porter Davis, Vol. 3327, The International Society for Optical Engineering, Bellingham, WA, 1998, pp. 44–60.

[4]Lesieutre, G. A., and Lee, U., "A Finite Element for Beams Having Segmented Active Constrained Layers with Frequency-Dependent Viscoelastic," *Smart Materials and Structures*, Vol. 5, No. 5, 1996, pp. 615–627.

[5]Nath, S., and Wereley, N., "Active Constrained Layer Damping for Rotorcraft Flex Beams," *Proceedings of the 36th AIAA/ASME/ASCE/AHS/ASC Structures, Structural Dynamics, and Materials Conference and Exhibit, and AIAA/ASME/AHS Adaptive Structures Forum*, April 1995, pp. 2867–2875; also AIAA Paper 95-1100, April 1995.

[6]Alam, A. B., Wang, K. W., and Gandhi, F., "Optimization of Enhanced Active Constrained Layer Treatment on Helicopter Flexbeams for Aeromechanical Stability Augmentation," *Smart Materials and Structures*, Vol. 8, No. 2, 1999, pp. 182–196.

[7]Hurt, M. K., and Wereley, N. M., "Controllable Fluid Dampers for Helicopter Rotor Stability Augmentation," *Proceedings of the 37th AIAA/ASME/ASCE/AHS/ASC Structures, Structural Dynamics, and Materials Conference and Exhibit, and AIAA/ASME/AHS Adaptive Structures Forum*, April 1996, pp. 247–238; also AIAA Paper 96-1294, April 1996.

[8]Kamath, G. M., and Wereley, N. M., "Characterization of Magnetorheological Helicopter Lag Dampers," *Journal of the American Helicopter Society*, Vol. 44, No. 3, 1999, pp. 234–248.

[9]Kamath, G. M., and Wereley, N. M., "Distributed Damping of Rotorcraft Flexbeams Using Electrorheological Fluids," *Proceedings of the 36th AIAA/ASME/ASCE/AHS/ASC Structures, Structural Dynamics, and Materials Conference and Exhibit, and AIAA/ASME/AHS Adaptive Structures Forum*, April 1995, pp. 2297–2307; also AIAA Paper 95-1082, April 1995.

[10]Kang, H., "Helicopter Blade Lag Damping Using Embedded Absorber," Ph.D. Dissertation, Dept. of Aerospace Engineering, Pennsylvania State Univ., University Park, Aug. 2001.

[11]Zapfe, J., and Lesieutre, G. A., "Broadband Vibration Damping in Beams Using Distributed Viscoelastic Tuned Mass Absorbers," *Proceedings of the 37th AIAA/ASME/ASCE/AHS/ASC Structures, Structural Dynamics, and Materials Conference and Exhibit, and AIAA/ASME/AHS Adaptive Structures Forum*, April 1996, pp. 2427–2436; also AIAA Paper 96-1595, April 1996.

[12]Hebert, C., and Lesieutre, G. A., "Rotorcraft Blade Lag Damping Using Highly Distributed Tuned Vibration Absorbers," *Proceedings of the 39th AIAA/ASME/ASCE/AHS/ASC Structures, Structural Dynamics, and Materials Conference and Exhibit, and AIAA/ASME/AHS Adaptive Structures Forum*, April 1998, pp. 2452–2457; also AIAA Paper 98-2001, April 1995.

[13]Bousman, W. G., "An Experimental Investigation of the Hingeless Helicopter Rotor-Body Stability in Hover," NASA TM-78489, June 1978.